Biomaterials Advances 188 (2026) 215015

Contents lists available at ScienceDirect

Biomaterials Advances

journal homepage: www.journals.elsevier.com/materials-science-and-engineering-c

Hydrogel microtumor arrays of patient melanoma recapitulate phenotypes and drug sensitivity

Yiling Liu [a,b], Matthew L. Pawlush [b], Justyna J. Gleba [b], Ella G. Lambert [c], Caitlin E. Williams [c], Martina H. Stenzel [a], John A. Copland [b,*], Kristopher A. Kilian [a,c,**]

[a] School of Chemistry, Australian Centre for NanoMedicine, University of New South Wales (UNSW), Sydney, New South Wales, Australia
[b] Department of Cancer Biology, Mayo Clinic Comprehensive Cancer Center, Jacksonville, FL, USA
[c] School of Materials Science and Engineering, University of New South Wales (UNSW), Sydney, New South Wales, Australia

ARTICLE INFO

Keywords:
Melanoma
Cancer stem cell
Hydrogel
Drug development
Patient derived xenograft

ABSTRACT

Patient-derived tumor xenograft (PDTX) models are considered the gold standard for preserving tumor heterogeneity and recapitulating patient drug responses, yet their use is limited by high cost, long timelines, and variable engraftment success. Here, we present the application of a soft lithography patterned polyacrylamide microtumor array platform designed to mimic biophysical aspects of the melanoma tumor microenvironment, including physiological stiffness, extracellular matrix (ECM) composition, and spatial confinement, which together recapitulate *in vivo* drug sensitivity for the evaluation of therapeutics. The microtumor array platform is comprised of approximately 100 distinct features per well, with a diameter of approximately 350 μm per feature, each imposing spatial confinement with peripheral geometric cues to confined cells. Using two $BRAF^{V600E}$ mutant melanoma cell lines, Mela14 (treatment-resistant) and Mela16 (treatment-naïve), we investigated whether microtumor arrays could restore cancer stem cell (CSC) characteristics, using ABCB5 and CD271 marker expression, and recapitulate PDTX drug response phenotypes to the BRAF/MEK inhibitor combination dabrafenib/trametinib (DT). Immunofluorescence analysis revealed that CSC marker expression was diminished on conventional tissue culture plastic (TCP) but restored to levels comparable to primary and PDTX tissue upon five days of spiral-patterned hydrogel confinement. Drug response assays demonstrated that microtumor array primed Mela14 cells retained DT resistance, whereas Mela16 cells remained responsive, paralleling PDTX outcomes. Global proteomics indicated that spiral confinement upregulated pathways in Mela14 associated with drug resistance, metastasis, cell repair and survival, while spiral patterned Mela16 showed upregulated pathways associated with cellular homeostasis and increased proteome plasticity. These findings suggest that polyacrylamide microtumor arrays can reproduce key features of the *in vivo* melanoma microenvironment, which may enable rapid, reproducible, and clinically relevant drug sensitivity testing. Therefore, this platform offers potential as a complementary preclinical model for personalized medicine and therapeutic discovery in cancer.

1. Introduction

Melanoma is a complex and heterogeneous disease driven by genetic mutations, epigenetic alterations, and microenvironmental factors. Mutations in oncogenes and tumor suppressor genes lead to uncontrolled cell proliferation, evasion of apoptosis, and resistance to therapy. Additionally, genomic instability and clonal evolution contribute to tumor heterogeneity, complicating treatment strategies. Recent advancements in sequencing technology and target identification have had a major diagnostic and treatment impact in the clinic. The widespread adoption of mutation identification technology has increased the prevalence of targeted therapies for melanoma, with drugs such as trametinib and dabrafenib, which have revolutionized treatment for patients with $BRAF^{V600E}$ mutations and aberrant MAPK pathway activity, improving disease outcomes and broadening treatment options [1]. While advances in sequencing technology and target identification have

* Corresponding author.
** Correspondence to: K.A. Kilian, School of Chemistry, Australian Centre for NanoMedicine, University of New South Wales (UNSW), Sydney, New South Wales, Australia.
E-mail addresses: copland.john@mayo.edu (J.A. Copland), k.kilian@unsw.edu.au (K.A. Kilian).

https://doi.org/10.1016/j.bioadv.2026.215015
Received 3 March 2026; Received in revised form 1 June 2026; Accepted 12 June 2026
Available online 17 June 2026

had a major impact, progression free survival is only observed in 19% of patients after 5 years when diagnosed with late-stage disease [2].

A key aspect of successful therapeutic development is the establishment of accurate and reproducible pre-clinical models. The field remains heavily reliant on animal models, particularly rodent models, to examine the effect of novel and combinatorial therapeutics. Rodent models remain one of the most sophisticated representation of human disease, with the most commonly employed being heterologous models, patient-derived tumor xenografts (PDTX), cell line xenografts, and autochthonous models or syngeneic tumor models, including genetically engineered models (GEM) [3]. PDTX have often been applied to melanoma research for their ability to recapitulate the complex melanoma microenvironment, retaining the biological and molecular features of melanoma tissue [4].

Currently, PDTX models are regarded as the gold standard preclinical model for their ability to retain a patient's genomic features, spatial structure and tumor heterogeneity [5]. One such feature is a population of cancer stem cells (CSCs), also commonly referred to as melanoma initiating cells (MICs), which are a subset of cells characterized by their ability to self-renew, reinitiate melanoma and reconstruct tumors, resulting in disease recurrence and resistance [6]. It has been shown that soft matrices, similar to the stiffness experienced by cancer cells *in vivo*, can enhance a CSC phenotype with cells reprogramming to adapt to environmental changes [7–9].

However, PDTX can have highly unpredictable variability with successful engraftments. Various factors are cited as potential reasons for engraftment failures, including the quality of the tumor sample, selection of engraftment site, unexpected death of primary recipient animal, and method of engraftment [10,11]. Other challenges present after successful engraftment can include loss of heterogeneity, selection bias, stroma replacement, tumor microenvironment changes, host cell carryover and contaminations, human-to-host cell oncogenic transformation, human and host viral infections, and immunological limitations [12]. These challenges highlight the complexities of maintaining tumor heterogeneity and microenvironmental interactions in experimental models, necessitating alternative approaches for more human physiologically relevant studies. There is demand for improved non-animal models that feature patient-derived materials, support features of *in vivo* tissue, with scope for use in personalized medicine by evaluating patient sensitivity to standard of care and experimental therapies. Thus, there is a need for preclinical models that (i) use patient-derived cells, (ii) preserve native heterogeneity and CSC populations, and (iii) are compatible with high-throughput drug testing.

As an alternative to PDTX models, the culture of patient-derived cells on tissue culture plastic (TCP) has numerous advantages with respect to simplicity and ease of analysis. However, patient materials often fail to attach and survive under these conditions and the cells lose key phenotypic features during culture that may be critical in understanding patient disease [13–15]. This attrition is largely driven by the absence of the native extracellular matrix and stromal support, which triggers cell death and selects only for the most robust, highly proliferative subpopulations. Over time, this artificial selection results in genetic drift and the loss of inherent tumor heterogeneity, ultimately yielding a homogenized cell line that bears limited resemblance to the original patient's pathology [16,17]. Engineered biomaterials that can mimic human physiology *in vitro* are highly desirable as they can more rapidly model patient disease and recapitulate patient drug responses. These models are typically 3D and generally fall into the categories of porous solid scaffolds, which provide structural support and defined pore architectures for nutrient transport; hydrogels, which offer tunable stiffness and high water content to mimic the soft tissue extracellular matrix; and decellularized extracellular matrix (dECM) scaffolds, which retain native biochemical cues and ultrastructure [18–21]. In melanoma, 3D scaffold free spheroids have been shown to have greater drug resistance compared to 2D TCP cultures and multicomponent cell models have been developed for further downstream applications [22,23]. Nevertheless, 3D bioengineered models will often fail in recapitulating patient disease states, and maintain a degree of cellular heterogeneity and materials complexity, which impedes their translation to preclinical screening pipelines.

As a middle ground between PDTXs and 3D spheroid models, hydrogel micropatterning to create microtumor arrays has proved a versatile “pseudo-3D” alternative, where key aspects of tissue can be maintained, *e.g.*, matrix stiffness, composition and tissue geometry, while providing spatially addressable arrays of microtumors for ease of data acquisition and analysis. Lee et al. showed how micropatterned melanoma cells respond to both substrate stiffness and geometric confinement, which led to the identification of features that coordinate phenotype changes [22–24]. Liu et al. used the same platform to study how these biophysical cues influence nanoparticle therapeutic uptake, demonstrating a pronounced increase in uptake in the stem cell-like cells at the periphery [25]. This technique partitions heterogeneous cell states within controlled geometries, where boundary curvature can ‘prime’ stem-like, chemo-resistant phenotypes, which have the potential to provide a means to evaluate the therapeutic efficacy of one or more compounds in different populations with high reproducibility in the same platform.

In this paper we demonstrate how hydrogel micropatterning will nurture endogenous phenotypes in patient-derived cells, thereby more closely recapitulating the cell states observed in primary tissue and PDTX models. Using patient-derived melanoma tissue with varying sensitivity to BRAF and MEK inhibitors, we show how culture on TCP erased features of drug resistance. In contrast, cells cultured on the hydrogel microtumor array were shown to regain features of tumorigenicity, with recapitulation of the appropriate drug response observed in the PDTX models. Intriguingly, the observed spatial control of phenotype was evident in whole primary PDTX tissues, suggesting that geometry and stiffness may be at work coordinating phenotype plasticity in growing tumor tissue. Together, this platform provides proof-of-concept to an avenue for maintaining the tumorigenic features of patient tissue, with the objective of building a preclinical tool for developing individualized therapy, and future scope for optimizing drugs that target multiple phenotypes simultaneously to streamline efficacious drug selection for patients (Fig. 1).

2. Results and discussion

2.1. Assessing tumorigenic and drug-resistant states in primary patient tissue and PDTX

Previously, Harris et al. demonstrated the use of subcutaneous PDTX models of melanoma for drug development using $BRAF^{V600E}$ mutant patient cells with non-responsive (Mela14) and responsive (Mela16) characteristics to standard of care [24]. In these experiments, they demonstrated that both cell lines became responsive after culture on TCP, thereby losing their inherent drug sensitivity [24]. We reasoned that the degree of therapeutic responsivity would be related to characteristics of tumorigenicity; specifically, the expression of melanoma stem cell markers, such as ABCB5 and CD271 [25,26]. Primary patient tissue, PDTX tissue and cells cultured on TCP were formalin fixed and prepared into a tissue microarray. Sliced microtome sections were mounted and immunostained for ABCB5 and CD271. Immunofluorescence imaging and quantitation revealed high overall expression of ABCB5 and CD271 in the Mela14 primary patient tissue and Mela14 PDTX tissue. Of the samples, primary Mela14 tissue showed the highest expression, with a 13-fold increase of normalized mean fluorescence intensity in ABCB5 and a 3-fold increase of CD271 when compared to normal skin tissue. Primary Mela16 tissue showed a 3-fold increase of both ABCB5 and CD271 compared to normal skin tissue. Much of this expression is retained in PDTX tissue, with Mela14 PDTX and Mela16 PDTX tissue showing a 12-fold and 3-fold increase in ABCB5 and a 6-fold and 3-fold increase in CD271 when compared to normal skin tissue,

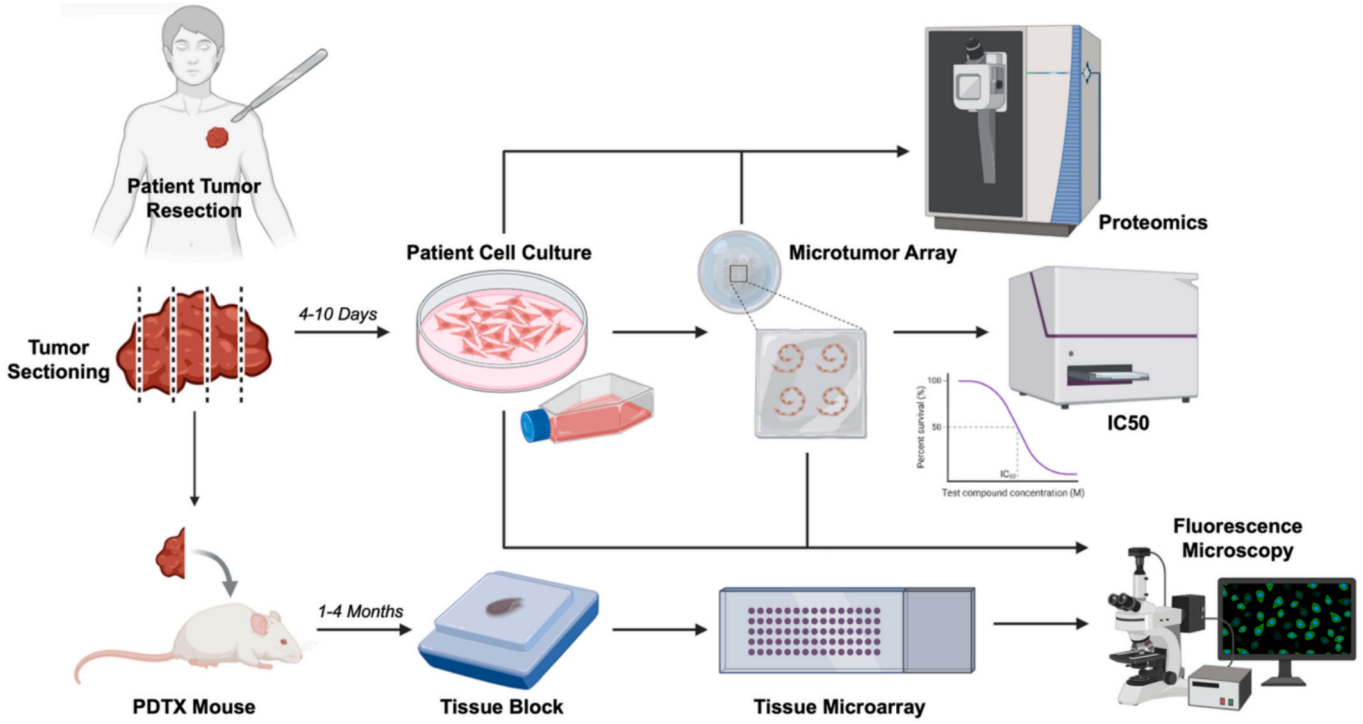

Fig. 1. Schematic of workflow. The patient's tumor is resected and sectioned into tumor pieces. A tumor piece was implanted subcutaneously into athymic nude female mice and collected at a size of approximately 150 mm^3. A separate tumor piece was diced and seeded onto tissue culture plastic. A monolayer culture was established, and the cells were then collected and seeded onto microtumor arrays.

respectively.

Interestingly, the Mela16 population did not show significant differences in expression of these markers irrespective of whether primary tissue, PDTX, or cultures on TCP. However, the Mela14 cells demonstrated a significant drop in expression of both markers when cultured on TCP, to levels comparable to the Mela16 TCP culture (Fig. 2). Normal skin tissue exhibited the lowest expression of both ABCB5 and CD271 compared to all samples. Taken together, the data suggest that the drug-resistant Mela14 cells are enriched for CSC markers in primary and PDTX tissue, but this enrichment is lost with extended TCP culture.

2.2. $BRAF^{V600E}$ mutant patient-derived melanoma cells under geometric confinement regain stem cell-like and drug-resistant phenotypes

Previous work by Lee et al. and Liu et al. demonstrated how micropatterned hydrogels could reprogram melanoma cell lines to stem cell-like phenotypes [27–30]. To explore whether patient-derived cells of varying drug sensitivity might be amenable to geometric confinement, Mela14 and Mela16 cells were cultured on fibronectin conjugated microtumor arrays and compared to cells cultured on TCP. Spiral patterns on 10 kPa hydrogels were selected because the evolving curvature mimics the interfacial boundary at an invasive tumor surface with mechanical properties that align with malignant tissue [28,30]. Hydrogel stiffness and fibronectin conjugation were confirmed using shear rheology and immunolabelling with confocal imaging, respectively (Figs. S1 and S2). Through immunofluorescence imaging after five days of culture, we observed that ABCB5 and CD271 expression were highest in Mela14 cells confined to spiral patterns, with a modest increase in expression for the Mela16 cells confined to spiral patterns (Fig. 3). There was negligible expression of ABCB5 or CD271 in either cell line when cultured on TCP. Intriguingly, the same cells cultured under confinement on hydrogels show an increase in stem cell-like molecular markers with characteristics of spatial heterogeneity akin to what was observed in PDTX tissue.

To supplement the observed differences in molecular markers associated with a CSC state, Mela14 and Mela16 cells cultured on spiral patterns or on TCP were removed from the substrates and cultured for one week in tumorsphere forming media conditions. Brightfield analysis indicated that overall Mela14 cells showed greater tumor forming capacity compared to Mela16 cells, supporting greater tumorigenicity (Fig. S4). While the spiral patterned Mela16 cells showed comparable sizes and growth rates to cells grown on TCP, the spiral patterned Mela14 population demonstrated a pronounced increase in growth rate and tumorsphere size, corroborating the enhanced stemness observed through ABCB5 and CD271 expression.

This method was shown to reproduce key features of the tumor microenvironment while maintaining a reproducible and spatially bounded format. The combination of matrix elasticity and interfacial geometry regulates cell state, predisposing subpopulations to adopt stem cell-like properties at the peripheral regions with higher geometric stress. There is increasing evidence that matrix mechanics regulates numerous pathways underlying tumor progression and drug sensitivity [31–33]. By culturing the cells on a physiologically representative stiffness with geometric confinement, promoting both cell-cell and cell-matrix signaling, the cellular aggregates experience cues which approximate those found *in vivo*. In this way, the confined cell populations express molecular markers and functional characteristics of tumorigenicity that align more closely with those of the original patient tumor when compared to standard culture on TCP [34]. It is plausible to speculate that these characteristics share similarities with the invasive niche observed *in vivo* [35,36]; however, additional experimentation is needed to establish quantitative comparisons. Irrespective, the microtumor array platform provides a means to spatially organize heterogeneous cell populations using patient-derived material, which could serve as a tool to classify patient cells and develop therapies that disrupt key phenotypes. Table S1 summarizes the key benefits of using the microtumor array platform in comparison to PDTX and TCP models.

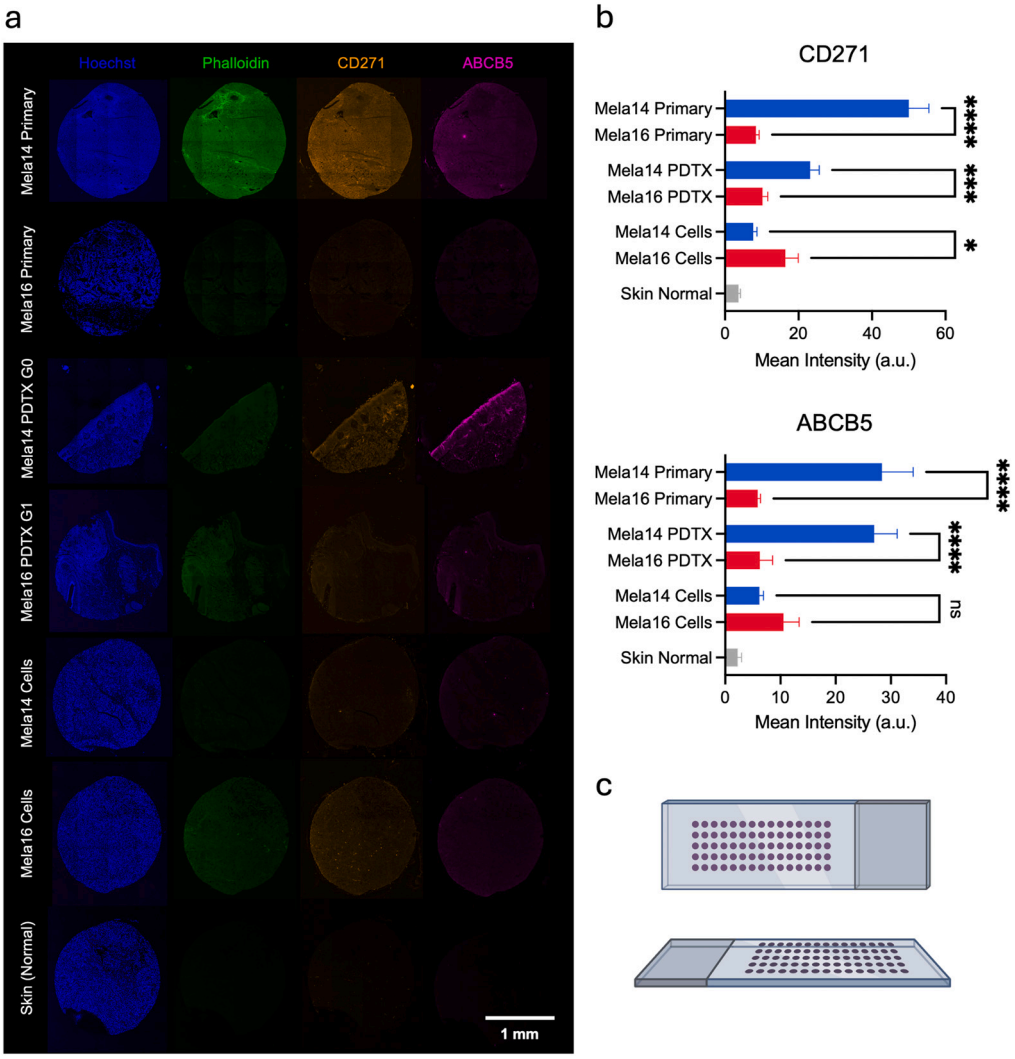

Fig. 2. Expression profile of ABCB5 and CD271 on Mela14 and Mela16 primary patient tissue, PDTX, TCP cells and normal skin tissue. a. Tissue microarray (1.5 mm histological cores) stained with Hoechst (Nuclei), Phalloidin (F-actin), CD271 (555 nm) and ABCB5 (647 nm). The scale bar is 1 mm. b. Quantified mean intensity expression of CD271 and ABCB5 in primary, PDTX, TCP cells and normal skin tissue. ****: $P \leq 0.0001$, ***: $P \leq 0.001$, *: $P \leq 0.05$. c. Tumor microarray schematic, samples were uniformly punched with 1.5 mm cores.

2.3. PDTX targeted therapy responses are recapitulated in microtumor arrays

The combination therapy dabrafenib used with trametinib (DT) was granted accelerated approval from the FDA for $BRAF^{V600E}$ mutated unresectable or metastatic solid tumors, including melanoma, supported by the COMBI-v and COMBI-d clinical trials and is currently the standard of care for unresectable Stage III and Stage IV melanoma [37–40]. In previous work, Harris et al. demonstrated that Mela14 and Mela16 PDTX recapitulated the respective patient responses: treatment with DT showed that Mela16 PDTX was responsive and Mela14 PDTX was unresponsive [24]. Having demonstrated that the geometric micropatterns on hydrogels recaptured key phenotypes in both patient-derived cell populations, we evaluated the microtumor array for assessing drug sensitivity in Mela14 and Mela16 cells exposed to DT combination therapy. After five days of culture on spiral microtumor arrays, the cells were collected and reseeded at 5000 cells/well to ensure equal seeding density between all populations and to remove the cells attached to the well plate from analysis. To confirm the viability of this approach we monitored ABCB5 expression, which indicated complete retention in expression for the timeframe of the drug assay (Fig. S3). After 72 h of treatment with DT, Mela14 cells showed decreased sensitivity compared to Mela16 cells, which remained responsive to the treatment (Fig. 4). Comparing the concentration on the dose-response curve where the DT combinatorial drug effect reaches its maximum, Mela14 cultured in spiral patterns showed a 4-fold increase in viability compared to cells cultured on TCP. This was not observed in Mela16, where no significant change was observed between the conditions. The sensitivity order matched the responses of the PDTX mouse models from Harris et al. and suggests the microtumor array system can restore drug sensitivity in a population of patient-derived cells. Clinical data for the individual where Mela14 cells were derived demonstrated non-responsive traits following BRAF kinase inhibitor treatment, ultimately succumbing to metastatic disease within three months of primary tumor resection [24]. While treatment of Mela14 cells on TCP with DT therapy showed responsivity, the Mela14 cells cultured on microtumor arrays mirrored clinical data with a resistant phenotype. Therefore, we propose that this platform may find utility in pre-screening therapeutic regimens to gauge responsivity and resistance prior to treatment.

In summary, the DT IC_{50} for cells cultured on the hydrogel microtumor array paralleled the response observed in PDTX mice. Mela14 in the microtumor array was resistant to DT treatment, whereas Mela16 in the microtumor array remained responsive to treatment. On TCP, both Mela14 and Mela16 cells show responsiveness to DT treatment.

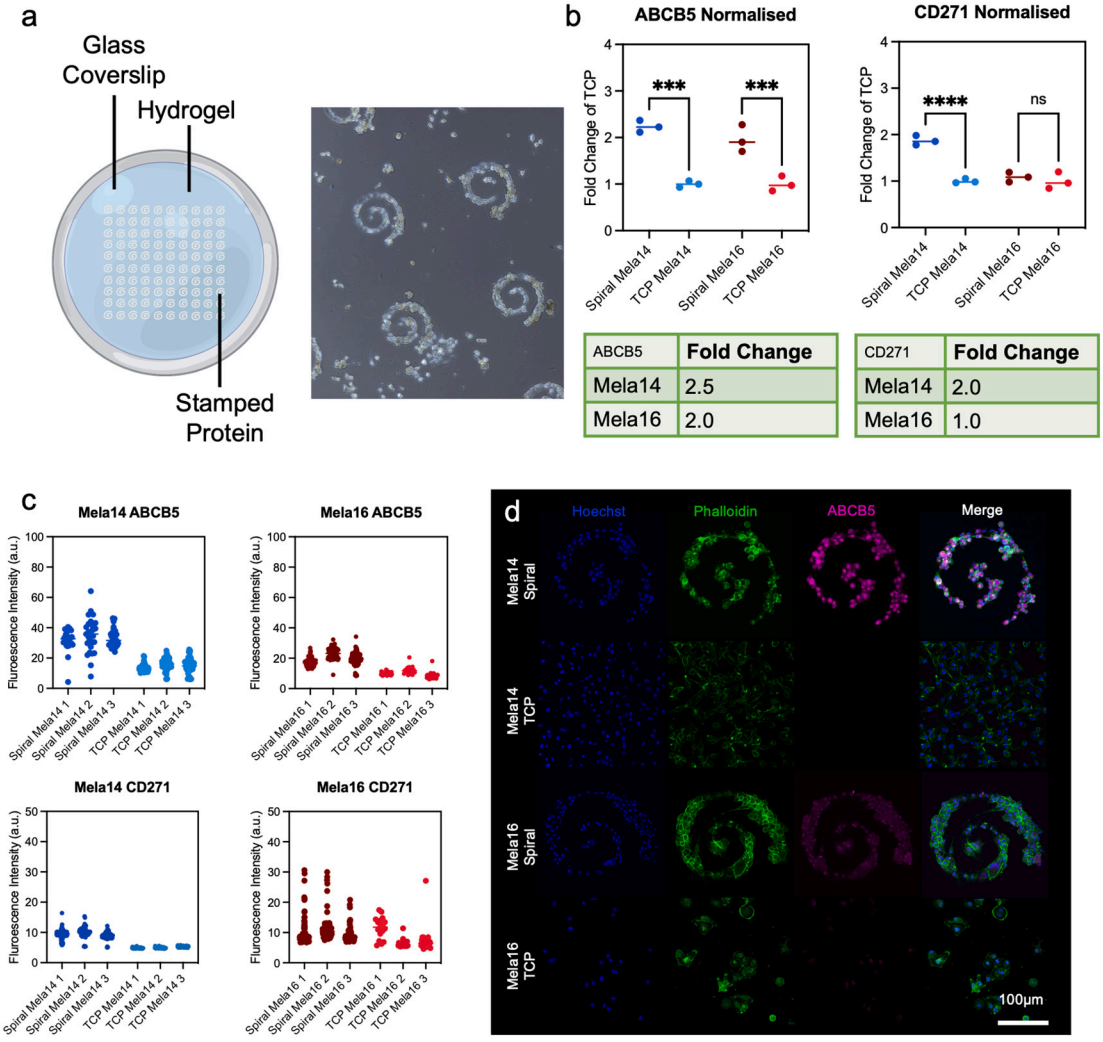

Fig. 3. Expression of ABCB5 and CD271 markers in Mela14 and Mela16 cell lines on spiral patterned hydrogels and TCP. a. Schematic of microcontact printed polyacrylamide hydrogel and representative light microscopy image of spiral confined Mela14 cells, each motif is 350 μm from the furthest points. b. Normalized expression and fold change of ABCB5 and CD271. ****: $P \leq 0.0001$, ***: $P \leq 0.001$. c. Scatter plot of ABCB5 and CD271 fluorescence intensity on spiral patterned hydrogels and TCP replicates. d. Representative fluorescence images of Mela14 and Mela16 after 5 days of culture on either spiral confined polyacrylamide hydrogels or TCP. Fluorescence channels present cancer cell nuclei (Hoechst), F-actin (488 Phalloidin), putative CSC marker ABCB5 (Alexa Fluor 647, magenta). (For interpretation of the references to color in this figure legend, the reader is referred to the web version of this article.)

Together, these findings demonstrate how microtumor arrays can better recapitulate key features observed in PDTX, compared to traditional culture on TCP, with evidence for correspondence to patient clinical outcome. The enriched ABCB5 and CD271 populations correspond to increased drug resistance, providing support for these molecular markers serving as indicators of both stemness and chemoresistance in melanoma.

2.4. Culture on microtumor arrays promotes the regulation of pathways associated with cell repair and drug resistance

To further investigate the changes induced by culture under hydrogel confinement, we evaluated protein expression patterns in Mela14 and Mela16 cells. Overall, confinement on hydrogels led to fewer total proteins identified in both lines. Mela16 exhibited a larger fraction of differentially expressed proteins than Mela14 (Table 1). The highest number of proteins was identified in Mela14 cultured on TCP (2664), followed by Mela14 cultured in spiral patterns (2511), then Mela16 cultured on TCP (2141), and the lowest number of proteins was in Mela16 cultured in spiral patterns (1911). A greater number of proteins identified may indicate an increase in protein diversity and, potentially, proteome complexity.

Mela14 exhibits a higher proteome similarity (88%) between TCP and spiral confinement culture than Mela16 (70%), which may reflect different levels of adaptability to the imposed mechanical microenvironment. Gene ontology (GO) analysis of proteins unique to Mela14 cells cultured in spiral patterns indicates a high fold enrichment of cell repair and apoptotic resistance pathways, which supports the increased resistance observed in drug response (Fig. 5.a) [41–43]. Molecular function analysis of both Mela14 and Mela16 cell lines with their respective conditions retained a similar frequency of proteins associated with each key biological cell function (Fig. 5.b). This indicates that all cells have preserved their core physiological and biological functions, demonstrating regulated cellular behavior. Differential expression analysis of the Mela14 cells indicated upregulation of proteins involved in cancer progression, metastasis and survival (ANXA2, TF3C1, Nup155, ACSL1, PBXIP1) [44–50] and downregulation of proteins involved in quiescence and apoptosis regulators (RS4X, HPRT1, VDAC2) [9,51–53]. Overall, proteomics analysis suggests that microconfinement does not overly perturb core cellular functions, with some evidence for the Mela14 cells displaying upregulation of pathways associated with tumorigenicity and malignant progression.

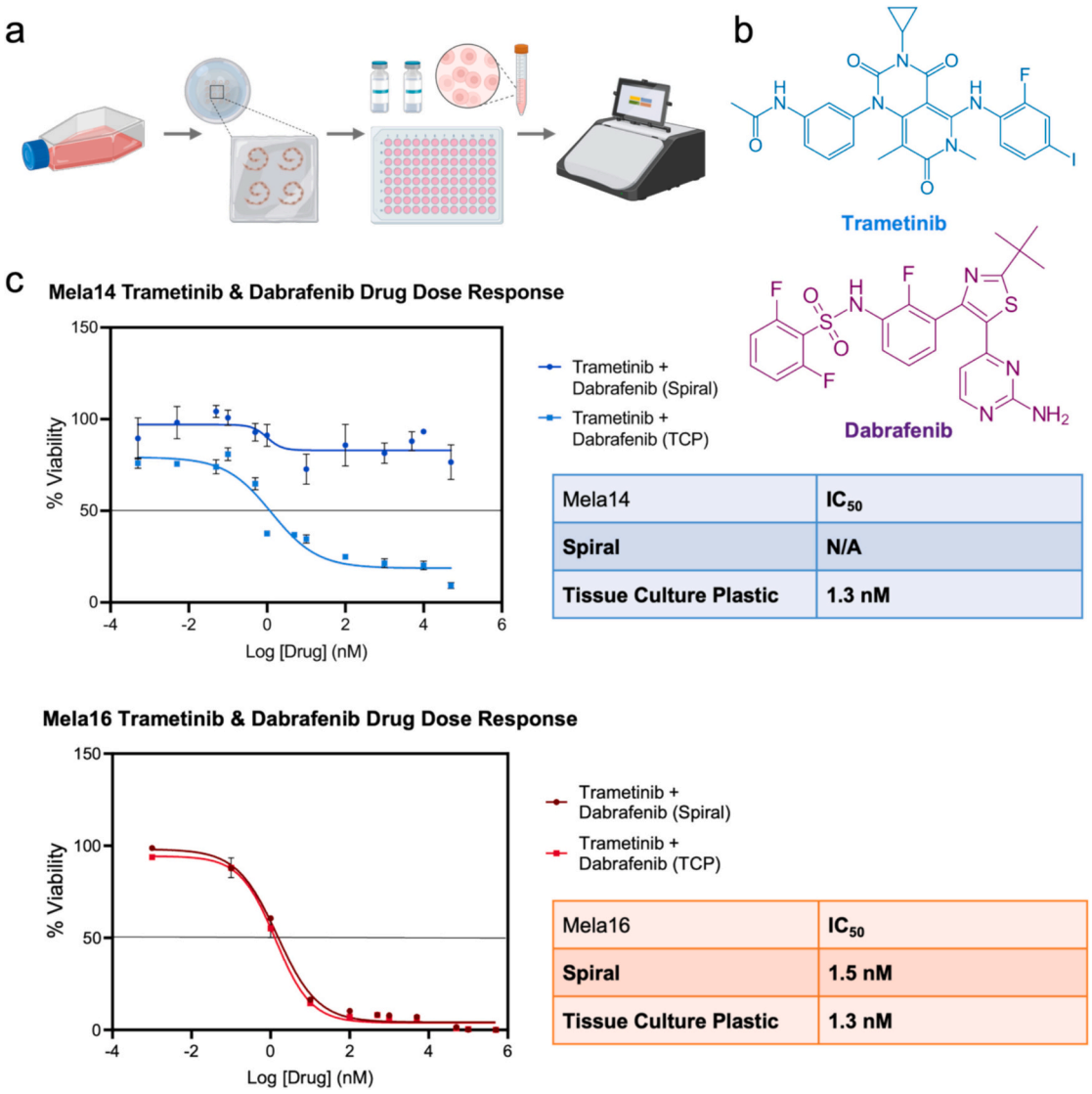

Mela14	IC_{50}
Spiral	**N/A**
Tissue Culture Plastic	**1.3 nM**

Mela16	IC_{50}
Spiral	**1.5 nM**
Tissue Culture Plastic	**1.3 nM**

Fig. 4. IC_{50} of dabrafenib and trametinib combinatorial therapy. a. Schematic detailing experimental protocol of IC_{50} assay-based study of DT combinatorial therapy. b. Chemical structure of dabrafenib and trametinib c. Drug responses of Mela14 and Mela16 cells primed with spiral pattern compared with cells from TCP. Results normalized to their respective DMSO-treated controls. Conditions classified as N/A do not reach 50% viability at any concentration up to 0.5 mM. Error bars represent standard deviation (±SD) with nonlinear regression curve fit.

Table 1
Total number of proteins identified in global proteomics and percentage similarity.

Sample	Total proteins identified	Sample	% similarity
Mela14 TCP	2664	Mela14 TCP & spiral	88.3
Mela16 TCP	2141	Mela16 TCP & spiral	70.1
Mela14 spiral	2511	Spiral Mela14 & Mela16	66.4
Mela16 spiral	1911	TCP Mela14 & Mela16	73.7

2.5. *Whole PDTX tissue shows features of stemness and tumorigenicity*

PDTX models, which involve engrafting a small section of patient tumor tissue subcutaneously, are the gold standard for preserving the histopathological characteristics, genomic and transcriptomic profiles, spatial heterogeneity, and patient-specific drug responses of cancers [54,55]. PDTX tissue produces a spatial distribution of cells and molecular markers within the tumor, offering critical insights into tumor heterogeneity and microenvironmental interactions [5]. While there is *in vitro* evidence that areas of high interfacial stress increase CSC expression, this is often only speculative with respect to *in vivo* contexts. Therefore, the spatial localization of CSCs within a PDTX tissue cross-section was evaluated to examine the interfacial boundary between the tumor and ECM *in vivo*, to evaluate whether molecular marker expression is correlative to DT treatment response. A similar display of CSC marker expression in the tumor tissue interfacing with the ECM may have significant implications for tumor prognosis and treatment, supporting the microtumor array model for evaluating patient tissue and drug responses..

Mela14, treatment resistant, and Mela16, treatment naïve, tissue was implanted subcutaneously into nude mice, and tumors were collected at the endpoint (5–6 weeks) with approximate dimensions of 15 × 15 × 15 mm. The tumor tissue was prepared as histological cross-sections before immunofluorescence staining with the CSC markers ABCB5 and CD271. Mela14 PDTX tumor tissue, which was interfacing with the ECM, exhibited approximately 3-fold higher expression of ABCB5 and CD271 (Fig. 6) compared to expression at the center of the tissue. PDTX from

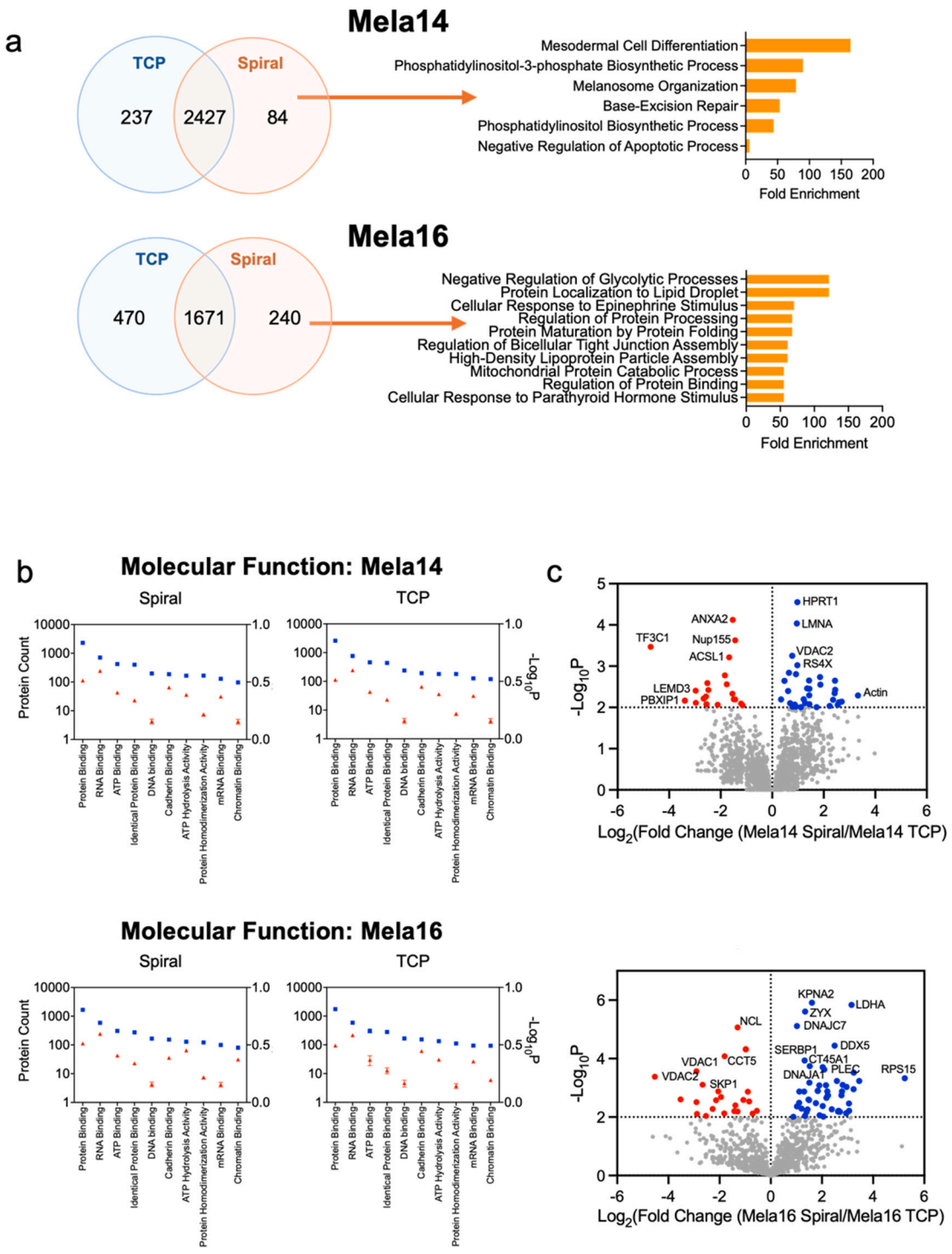

Fig. 5. Global proteomics of Mela14 and Mela16 on spiral patterns and TCP. a. Venn diagram comparing the number of identified proteins for Mela14 and Mela16 with $n = 3$ biological replicates. Proteins unique to spiral microtumor array and TCP from Mascot protein identification software. Functional annotation clustering of the enriched Gene Ontology (GO) terms in the biological process (BP) category was analyzed with DAVID Functional Annotation Bioinformatics Microarray Analysis and biological processes are ordered by fold change [1–3]. b. Molecular function representing protein count and -$\log_{10}$P value for top 10 molecular functions. c. Volcano plot for Mela14 and Mela16 indicating significantly differentially expressed proteins. The horizontal line shows p-value (nominal $p < 0.01$, FDR-adjusted) cut-off and vertical lines indicate significantly up/down-regulated proteins. Quantitation performed with Scaffold quantitative analysis setup. Statistical test performed are t-test with Benjamini-Hochberg correction.

Mela16 had overall lower expression of ABCB5 and CD271 when compared to Mela14 (Fig. 6). At the edge of the tumor, Mela14 exhibited a 5-fold increase in ABCB5 and 3-fold increase in CD271 expression when compared to Mela16, suggesting the drug resistant tissue has greater CSC characteristics at the tumor-matrix interfacial boundary.

This finding may have significant implications for tumor grading, prognosis and combinatorial drug development for malignant melanoma. Current therapeutic options for advanced disease are often limited due to the emergence of resistance, and patients whose tumors are incompatible with standard targeted regimens face poor prognoses

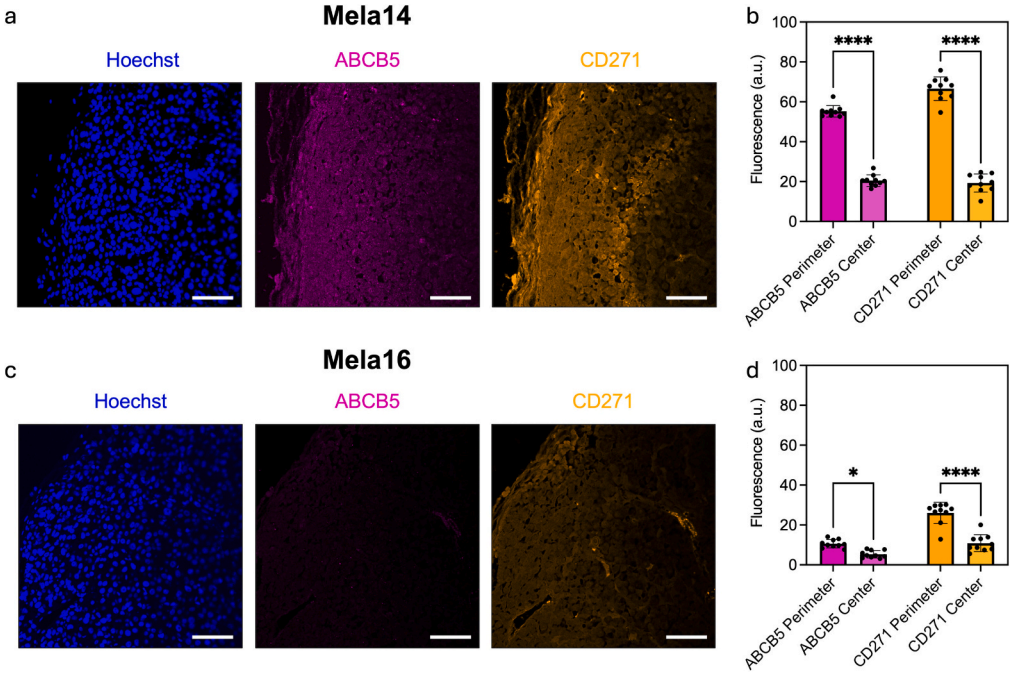

Fig. 6. Mela14 and Mela16 PDTX histological cross-section expression of ABCB5 and CD271 (20×). a. Immunofluorescence image of Mela14 PDTX histological cross-section. Fluorescence channel presents cell nuclei (Hoechst), ABCB5 (Alexa Fluor 647, Magenta) and CD271 (Alexa Fluor 555, Orange). The scale bar is 1 mm. b. Quantification of the Mela14 mean ABCB5 and CD271 intensity at the perimeter ($n = 10$) and centre (n = 10) of the tissue section. ****: $P \leq 0.0001$. c. Immunofluorescence image of Mela16 PDTX histological cross-section. Fluorescence channel presents cell nuclei (Hoechst), ABCB5 (Alexa Fluor 647, magenta) and CD271 (Alexa Fluor 555, orange). The scale bar is 1 mm. d. Quantification of the Mela16 mean ABCB5 and CD271 intensity at the perimeter (n = 10) and centre (n = 10) of the tissue section. ****: $P \leq 0.0001$, *: $P \leq 0.05$. (For interpretation of the references to color in this figure legend, the reader is referred to the web version of this article.)

and a lack of effective alternatives [56]. A promising avenue is to design therapeutic strategies that address CSC populations, which have been implicated in therapy resistance and tumor recurrence. The microtumor array platform offers a preclinical model to assess such approaches, enabling the evaluation of drug responses in CSC-enriched microenvironments with patient-derived cells. However, we acknowledge that this platform is unlikely to mimic all phenotype changes that occur between primary tissue and culture on TCP. Nevertheless, the ability to guide key phenotypic signatures corresponding to tumorigenicity and drug sensitivity has the potential to provide novel screening tools that obviate the loss of these features observed in standard tissue culture. Furthermore, the evidence for increased interfacial CSC populations *in vivo* suggests that geometric targeting may prove a viable therapeutic approach.

3. Conclusion

In this work, the application of polyacrylamide hydrogels, patterned through soft lithography to create uniform geometric protein microtumor arrays, has been shown to recapitulate features of native tumor tissue in patient-derived melanoma cultures. Mela14 and Mela16 primary patient-derived cells were spatially confined into spiral features on 10 kPa fibronectin patterned polyacrylamide hydrogel microtumor arrays. It was observed that the CSC markers ABCB5 and CD271 expression had increased when Mela14 and Mela16 cells were placed onto the microtumor arrays for five days, with comparable levels to the primary patient and PDTX tissue. Examination of DT drug response with the transformed cells was shown to recapitulate trends observed in PDTX mice, with Mela14 exhibiting DT resistance, whereas Mela16 remained responsive. Together, this platform provides proof-of-concept as a platform to maintain the tumorigenic features of patient tissue, with the objective of building a preclinical tool for individualized therapy development, and future scope for optimizing drugs that target multiple phenotypes simultaneously to streamline efficacious drug selection for patients.

These results show promise for the microtumor array platform to serve as a tool for personalized medicine, as the patients corresponding to the Mela14 and Mela16 cells had dramatically different clinical outcomes, while both being classified as clinically similar having the $BRAF^{V600E}$ mutation, prescribing similar first-line treatments. Prescreening therapeutics on the microtumor array using these individuals cells may have indicated the differences in drug sensitivity, thereby opening up alternative or complementary therapeutic options. With additional validation using a broader array of patient tissues, this platform could provide a simple and rapid method to examine whether a therapeutic will be effective, especially in cases where multiple treatment plans are under consideration. The microtumor array platform can also be readily and consistently modulated to change stiffness, microtumor shape and/or protein functionalization, and can be individually designed to match tissue *in situ*, providing an environment to nurture native characteristics. Considering the flexibility of the microtumor array system, future work could involve incorporation of stromal and immune cell populations, providing scope for development of combination therapies targeting different cell types in the tumor microenvironment.

4. Experimental

4.1. Materials and reagents

Antibodies

Reagent/resource	Source	Identifier	Dilution
Hoescht 33342	Biotium	#40047	1:1000
DAPI (1 mg/mL)	Thermo Scientific	62248	1:1000
Phalloidin CF488A	Biotium	#00042	1:250
Phalloidin-Atto 488	Sigma-Aldrich	49409	1:250

(*continued on next page*)

(*continued*)

Reagent/resource	Source	Identifier	Dilution
Primary			
Anti-p75 (CD271) NGF Receptor antibody [8J2], Mouse Monoclonal	Abcam	ab245134	1:250
ABCB5 Antibody - BSA Free, Rabbit Polyclonal	Novus Biologicals	NBP177687	1:500
Secondary			
Goat anti-Rabbit IgG (H + L) Highly Cross-Adsorbed Secondary Antibody, Alexa Fluor Plus 555	Invitrogen	A32732	1:250
Alexa Fluor 647 AffiniPure Goat Anti-Mouse IgG	Jackson ImmunoResearch	115-605-146	1:250
Anti-Mouse IgG (H + L), highly cross-adsorbed, *CF*™ 647 antibody produced in goat	Sigma-Aldrich	SAB4600183	1:250

Drugs

Reagent/resource	Source	Identifier
Dabrafenib	Selleckchem	S2807
Trametinib	Selleckchem	GSK1120212

Reagents

Reagent/resource	Source	Identifier
Dimethylsulfoxide (DMSO)	Sigma-Aldrich	D2650
CellTiter-Glo 3D Cell Viability Assay	Promega	G9681
Cell culture		
Dulbecco's Phosphate Buffered Saline (DPBS)	Corning	45000-434
DPBS, no calcium, no magnesium	Gibco	14190144
Normocin	InvivoGen	ant-nr-05
Fetal Bovine Serum, qualified	Gibco	26140079
MEM (Minimum Essential Medium) Nonessential Amino Acids, 100×	Corning	25-025-CI
HEPES (N-2-hydroxyethylpiperazine-N′-2-ethanesulphonic acid) Buffer 1 M Solution	Corning	25-060-CI
Antibiotic-Antimycotic (100×)	Gibco	15240062
Trypsin-EDTA (0.25%)	Gibco	25200072
TrypLE Express Enzyme (1×)	Gibco	12605010
Fixation/mounting		
Formalin Solution, 10% (Histological)	Fisher Scientific	SF984
16% Formaldehyde (w/v), Methanol-free	Pierce	28906
Xylenes, histological grade	Sigma-Aldrich	534056
Bovine serum albumin (BSA)	Sigma-Aldrich	A3294
Triton X-100	Thermo Scientific	A16046.AE
Tween™ 20	Thermo Scientific	85113
Alcohol, 70%, HistoPrep™	Fisher Scientific	HC-1000-1GL
ProLong™ Gold Antifade Mountant	Invitrogen	P36930
Polydimethylsiloxane (PDMS) stamp		
SYLGARD 184 Silicone Elastomer Kit	Dow	01673921
Polyacrylamide hydrogel		
N,*N*′-Methylenebis(acrylamide)	Sigma-Aldrich	146072
Acrylamide	Sigma-Aldrich	A3553
(3-Aminopropyl)triethoxysilane	Sigma-Aldrich	741442
Glutaraldehyde solution (Grade II, 25% in H_2O)	Sigma-Aldrich	G6257
Ammonium persulfate	Chem-Supply	AA019

(*continued on next column*)

(*continued*)

Reagent/resource	Source	Identifier
N,*N*,*N*′,*N*′-Tetramethylethylenediamine	Sigma-Aldrich	411019
Hydrazine hydrate (reagent grade, N_2H_4 50–60%)	Sigma-Aldrich	225819
Acetic acid	Sigma-Aldrich	695092
Sodium (meta)periodate	Sigma-Aldrich	S1878
Fibronectin Human Protein, Plasma	Gibco	33016015
Cell lysate preparation		
RIPA Lysis and Extraction Buffer	Thermo Scientific	89900
Protease Inhibitor Cocktail	cOmplete	11697498001

Products/consumables

Reagent/resource	Source	Identifier
Advanced PAP Pen (2 mm)	Sigma-Aldrich	Z672548
Costar 96-well Clear Round Bottom Ultra-Low Attachment Microplate	Corning	7007
96-well Black/Clear Round Bottom Ultra-Low Attachment Surface Spheroid Microplate	Corning	4520
Round cover glasses (18 mm)	Marienfeld	0111580
Fisherbrand™ InkJet Plus Microscope Slides	Fisher Scientific	12-550-111

4.2. Hydrogel fabrication

4.2.1. Polydimethylsiloxane stamp fabrication

Polydimethylsiloxane (PDMS) stamps were fabricated through polymerization on a silicon master patterned with photoresist, created using ultraviolet photolithography through a laser printed mask. An even layer of a 10:1 mixture of Polydimethylsiloxane elastomer base to crosslinker was poured onto the silicon master and placed into a degassing chamber until bubbles were removed. The PDMS was cured at 60 °C for 12 h, then detached from the master.

4.2.2. Polyacrylamide hydrogel synthesis and functionalization

10 kPa polyacrylamide hydrogels were fabricated on 18 mm glass coverslips following established protocols modified from Tse and Engler and Tang et al. [57,58]. To summarize, 18 mm round cover glasses were sonicated in ethanol, then Milli-Q water for 15 min each, then functionalized with 0.5% (3-aminopropyl)triethoxysilane, followed by 0.5% glutaraldehyde for 30 min, with three washes between each treatment. A polyacrylamide stock solution was prepared with 2.5 mL 40% acrylamide, 0.5 mL 2% *N*,*N*′-methylenebis(acrylamide) and 7 mL Milli-Q water, then degassed with argon for 15 min. The polymerization reaction was initiated by 5 μL ammonium persulfate and catalyzed by 0.5 μL tetramethylethylenediamine (TEMED) when added to the 500 μL acrylamide/bis-acrylamide stock solution. 20 μL of the prepolymerized solution was dispensed onto a hydrophobically treated glass slide, and the modified surface of the coverslip was placed on the droplet. After 15 min, the polyacrylamide hydrogel coated coverslip was gently detached from the hydrophobic glass slide.

Polyacrylamide hydrogels were functionalized with hydrazine hydrate for 30 min, then treated with 1% acetic acid for 1 h and rinsed three times with Milli-Q water between each treatment. The hydrazine modified hydrogels were left overnight at 4 °C in Milli-Q water before use.

4.2.3. Polyacrylamide hydrogel protein deposition

PDMS stamps were cleaned with 100% ethanol. Human plasma fibronectin was dispersed in Milli-Q water and oxidized with 0.35% (w/

v) sodium (meta)periodate for 45 min, then pooled onto the patterned surface of the stamps for 30 min. The stamp surface was gently dried with a stream of nitrogen gas to reveal a white fibronectin protein layer on the stamping surface. The oxidized fibronectin was transferred through contact printing onto the hydrazine modified polyacrylamide hydrogel, applying light pressure to ensure complete transfer. The fibronectin patterned hydrogels were stored in Milli-Q water at 4 °C until use.

4.3. Cell culture and maintenance

4.3.1. Mela14 and Mela16 cells

Cell lines were established in the Cancer Biology and Translational Research Laboratory at Mayo Clinic's campus in Florida by Dr. Copland and the research team. Tissue was resected or biopsied from the patient and proliferated on TCP to form a cell line. Detailed characterization of PDTX tissue and patient tissue are detailed in Harris et al. [24] Cell lines are validated through STR profiling against primary tissue.

Ethics approvals for all donated patient tissue were established at the Cancer Biology and Translational Research Laboratory at the Mayo Clinic in Florida. Development of patient-derived preclinical models and collection of patient tumor tissue were approved by the Mayo Institutional Review Board. PDTX were grown in athymic nude mice with adherence to the NIH Guide for the Care and Use of Laboratory Animals and approved by Institutional Animal Care and Use Committee (ASP #: 980702).

4.3.2. Mela14 and Mela16 cell culture

Cultures were maintained in high glucose DMEM media supplemented with 5% FBS, 1% PSA, 1% HEPES, 1% MEM, and 0.2% Normocin. Cells were seeded onto TCP or micropatterned polyacrylamide hydrogels at 10,000 cells/mL, 1 mL per well, and cultured for 5 days to form microtumor arrays.

4.3.3. Tumorsphere assay

Cells were manually dislodged from their microtumor array or TCP surfaces (enzyme-free) and seeded into the serum-free media (R&D Systems™ StemXVivo Serum-Free Tumorsphere Media, Cat. Number CCM012) at 3000 cells/well in a 96-well ultra-low attachment flat bottom plate. Tumorsphere number and area was monitored through brightfield microscopy and quantified using FIJI.

4.3.4. PDTX model

Donated patient tumor tissue was sectioned to approximately 3 × 3 × 3 mm pieces and implanted subcutaneously into the lower back of athymic nude female mice (5–6 weeks of age). Tumor growth was monitored weekly with calipers, and engraftment was considered successfully developing when the implanted tumor reached a minimum volume of 150 mm^3. A tumor size of approximately 15 × 15 × 15 mm was considered the endpoint. Human-specific Lamin A/C immunohistochemistry was used to confirm the presence of human cells in PDTX tumors.

4.3.5. Cell counting

Cell number for all resuspended samples was determined with the Countess 3 Automated Cell Counter with Countess Cell Counting Chamber Slides (Invitrogen).

4.4. Immunofluorescence staining and imaging

4.4.1. Cell fixation

Cell samples were fixed with 4% paraformaldehyde (PFA)/10% formalin for 30 min. Samples were washed with DPBS three times. Permeabilization was performed with 0.1% Triton X-100 in DPBS for 30 min, then blocked with 1% BSA in DPBS for 15 min. The sample was stored in 1% BSA in DPBS until primary staining.

4.4.2. Paraffin blocked tissue slide staining

Protocol adapted from Zaqout, S.; Becker, L. L.; Kaindl, A. M., Immunofluorescence Staining of Paraffin Sections Step by Step. *Frontiers in Neuroanatomy* 2020, *14* [59].

In summary, to dewax the paraffin slide, the slide was submerged in xylene for 1 h, then 1:1 xylene: ethanol for 5 min, ethanol for 5 min, 1:1 ethanol: Milli-Q water for 5 min, and finally, Milli-Q water for 5 min. For permeabilization, the slides were rinsed with DPBS twice for 10 min and then 0.25% Triton X-100 (v/v) in DPBS for 10 min. Blocking was performed with 5% BSA in DPBS. All steps were completed in a vertical staining jar. Slides were removed before staining, and a hydrophobic barrier was made around the sample with a PAP pen.

4.4.3. Primary stain

ABCB5 (1:500) and CD271 (1:250) in 1% BSA in DPBS were added to cover the sample surface for 1 h (RT). Samples were washed twice with 1% BSA in DPBS.

4.4.4. Secondary stain

Hoechst 33342 (1:1000), Alexa Fluor 488 Phalloidin (1:200), Alexa Fluor 555 anti-Rabbit Secondary Antibody (1:250) and Alexa Fluor 647 anti-Mouse Secondary Antibody (1:250) in 1% BSA in DPBS were added to cover the sample surface for 1 h (RT) in the dark. Samples were mounted with ProLong™ Diamond Antifade Mountant and set overnight (RT) prior to imaging.

4.4.5. Confocal imaging

All confocal images were collected on the Zeiss LSM 880 Confocal Laser Scanning Microscope with Zen Black software.

4.4.6. Wide-field imaging

All widefield images were collected on Keyence BZ-X810 with filter cubes, BZ-X Filter DAPI (OP-87762), BZ-X Filter GFP (OP-87763) and BZ-X Filter TexasRed (OP-87765) and stitched with Keyence Advanced Analysis Software.

4.4.7. Drug dose response: IC_{50}

IC_{50} studies were conducted using CellTiter-Glo 3D Cell Viability Assay in accordance with the corresponding technical manual protocol, and luminescence signal was collected on Promega GloMax 96 Microplate Luminometer. Cells were cultured on microtumor arrays for 5 days, then reseeded at 5000 cells/well into a 96-well plate. Cells were allowed to reattach overnight and treated with varying concentrations of dabrafenib and trametinib at a 10-fold dilution factor scale. After 72 h of treatment, CellTiter-Glo 3D reagent was added at a 1:1 ratio of media within each well. The plate was incubated at RT in the dark for 30 min, and luminescence signal was collected with parameters of wavelength range between 350 and 700 nm and integration time of 500 ms.

4.4.8. Global proteomics

Mela14 and Mela16 cells were collected through physical removal after 5 days on either polyacrylamide hydrogel spiral patterns or tissue culture flasks. The cells were lysed using 50–100 μL RIPA buffer and protease inhibitor cocktail, approximately 1.5× cell pellet volume, then frozen to −80 °C. The Pierce BCA Protein Assay Kit was used to calculate protein concentrations. All samples were diluted to 50 μg of protein and underwent enzyme digestion with trypsin.

Electrospray ionization quadrupole time-of-flight mass spectrometry was performed on Orbitrap Exploris 480 Mass Spectrometer. Charge state deconvolution and deisotoping were not performed. All MS/MS samples were analyzed using Mascot (Matrix Science, London, UK; version 2.8.3). Mascot was set up to search the SProt database (selected for *Homo sapiens*, 20488 entries) with the digestion enzyme trypsin. Mascot was searched with a fragment ion mass tolerance of 0.050 Da and a parent ion tolerance of 5.0 PPM. Oxidation of methionine and carbamidomethyl of cysteine were specified in Mascot as variable

modifications.

Scaffold (version Scaffold 5.3.3, Proteome Software Inc., Portland, OR) was used to validate MS/MS based peptide and protein identifications. Peptide identifications were accepted if they could be established at greater than 80.0% probability by the Peptide Prophet algorithm with Scaffold delta-mass correction [60]. Protein identifications were accepted if they could be established at greater than 80.0% probability and contained at least 2 identified peptides. Protein probabilities were assigned by the Protein Prophet algorithm [61]. Proteins that contained similar peptides and could not be differentiated based on MS/MS analysis alone were grouped to satisfy the principles of parsimony. Proteins were annotated with GO terms from NCBI [43].

4.5. Data and statistical analysis

4.5.1. Microscopy data analysis

Confocal images were quantified using MATLAB script developed by Katharina Gaus Light Microscopy Facility at UNSW Sydney.

4.5.2. Statistical analysis

GraphPad Prism (version 10.3.1) was used for statistical analysis of all data unless otherwise specified. Data is presented as the mean, and error bars denote ± standard deviation unless otherwise specified. Statistical significance of two sample groups was calculated using a two-tailed unpaired *t*-test unless specified otherwise. Differences were considered significant when $p < 0.05$. Statistical significance of three sample groups or more was calculated using a one-way ANOVA with no matching or pairing. All experiments were performed with $n = 3$ biological replicates.

CRediT authorship contribution statement

Yiling Liu: Writing – original draft, Methodology, Investigation, Formal analysis. **Matthew L. Pawlush:** Visualization, Methodology, Data curation. **Justyna J. Gleba:** Visualization, Methodology, Data curation. **Ella G. Lambert:** Data curation, Formal analysis, Investigation. **Caitlin E. Williams:** Data curation, Formal analysis, Resources. **Martina H. Stenzel:** Writing – review & editing, Supervision, Conceptualization. **John A. Copland:** Supervision, Resources, Project administration, Conceptualization. **Kristopher A. Kilian:** Writing – review & editing, Supervision, Project administration, Funding acquisition, Conceptualization.

Declaration of competing interest

The authors declare that they have no known competing financial interests or personal relationships that could have appeared to influence the work reported in this paper.

Acknowledgements

Y.L. acknowledges the scholarship support from the Australian Government Research Training Program and Fulbright Future Scholarship (Postgraduate), funded by the Kinghorn Foundation. Y.L. also acknowledges the Mayo Clinic College of Medicine and Science Visiting Graduate Student Program. This work was funded by the National Cancer Institute of the National Institutes of Health Cancer Tissue Engineering Collaborative (C-TEC) program (R01CA251443, K.A.K., J.A.C.), the National Health and Medical Research Council (APP1185021, K.A.K.) and the Mayo Clinic (90078999, J.A.C.). Tissue slices were prepared by Brandy H. Edenfield at the Mayo Clinic Research Core Facility. Global proteomics was performed by Dr. Ling Zhong at the Bioanalytical Mass Spectrometry Facility (BMSF) at UNSW, Sydney. We acknowledge and thank them for their contribution to this work.

Appendix A. Supplementary data

Supplementary data to this article can be found online at https://doi.org/10.1016/j.bioadv.2026.215015.

Data availability

Data will be made available on request.

References

[1] G.V. Long, A. Hauschild, M. Santinami, J.M. Kirkwood, V. Atkinson, M. Mandala, B. Merelli, V.C. Sileni, M. Nyakas, A. Haydon, C. Dutriaux, C. Robert, L. Mortier, J. Schachter, D. Schadendorf, T. Lesimple, R. Plummer, J. Larkin, M. Tan, S. B. Adnaik, P. Burgess, T. Jandoo, R. Dummer, Final results for adjuvant dabrafenib plus trametinib in stage III melanoma, N. Engl. J. Med. 391 (18) (2024) 1709–1720.

[2] A. Knight, L. Karapetyan, J.M. Kirkwood, Immunotherapy in melanoma: recent advances and future directions, Cancers (Basel) 15 (4) (2023).

[3] S.I. De Vleeschauwer, M. van de Ven, A. Oudin, K. Debusschere, K. Connor, A. T. Byrne, D. Ram, A.M. Rhebergen, Y.D. Raeves, M. Dahlhoff, V. Dangles-Marie, E. R. Hermans, OBSERVE: guidelines for the refinement of rodent cancer models, Nat. Protoc. 19 (9) (2024) 2571–2596.

[4] A.M.E. Abdalla, L. Xiao, M.W. Ullah, M. Yu, C. Ouyang, G. Yang, Current challenges of cancer anti-angiogenic therapy and the promise of nanotherapeutics, Theranostics 8 (2) (2018) 533–548.

[5] Y. Liu, W. Wu, C. Cai, H. Zhang, H. Shen, Y. Han, Patient-derived xenograft models in cancer therapy: technologies and applications, Signal Transduct. Target. Ther. 8 (1) (2023) 160.

[6] N. Nguyen, K.L. Couts, Y. Luo, M. Fujita, Understanding melanoma stem cells, Melanoma Manag. 2 (2) (2015) 179–188.

[7] B. Tian, Q. Luo, Y. Ju, G. Song, A soft matrix enhances the cancer stem cell phenotype of HCC cells, Int. J. Mol. Sci. 20 (11) (2019).

[8] J. Lv, Y. Liu, B. Huang, Mechanical softness: a true stemness feature for cancer cells, Mol. Cell. Oncol. 8 (2) (2021) 1882285.

[9] K. Chen, C. Zhang, S. Ling, R. Wei, J. Wang, X. Xu, The metabolic flexibility of quiescent CSC: implications for chemotherapy resistance, Cell Death Dis. 12 (9) (2021) 835.

[10] J. Lee, G. Lee, H.S. Park, B.-K. Jeong, G. Gong, J.H. Jeong, H.J. Lee, Factors associated with engraftment success of patient-derived xenografts of breast cancer, Breast Cancer Res. 26 (1) (2024) 49.

[11] C. Chen, W. Lin, Y. Huang, X. Chen, H. Wang, L. Teng, The essential factors of establishing patient-derived tumor model, J. Cancer 12 (1) (2021) 28–37.

[12] J. Jin, K. Yoshimura, M. Sewastjanow-Silva, S. Song, J.A. Ajani, Challenges and prospects of patient-derived xenografts for cancer research, Cancers (Basel) 15 (17) (2023).

[13] M. Richter, O. Piwocka, M. Musielak, I. Piotrowski, W.M. Suchorska, T. Trzeciak, From donor to the lab: a fascinating journey of primary cell lines, Front. Cell Dev. Biol. 9 (2021) 711381.

[14] F. Rambow, J.C. Marine, C.R. Goding, Melanoma plasticity and phenotypic diversity: therapeutic barriers and opportunities, Genes Dev. 33 (19–20) (2019) 1295–1318.

[15] Y. Fu, B.L. Khoo, C.T. Lim, Advancements and challenges in culturing patient-derived cancer cells for personalized therapeutics, Front. Lab Chip Technol. 4 (2025) (2025).

[16] U. Ben-David, B. Siranosian, G. Ha, H. Tang, Y. Oren, K. Hinohara, C.A. Strathdee, J. Dempster, N.J. Lyons, R. Burns, A. Nag, G. Kugener, B. Cimini, P. Tsvetkov, Y. E. Maruvka, R. O'Rourke, A. Garrity, A.A. Tubelli, P. Bandopadhayay, A. Tsherniak, F. Vazquez, B. Wong, C. Birger, M. Ghandi, A.R. Thorner, J.A. Bittker, M. Meyerson, G. Getz, R. Beroukhim, T.R. Golub, Genetic and transcriptional evolution alters cancer cell line drug response, Nature 560 (7718) (2018) 325–330.

[17] M. Kapałczyńska, T. Kolenda, W. Przybyła, M. Zajączkowska, A. Teresiak, V. Filas, M. Ibbs, R. Bliźniak, Ł. Łuczewski, K. Lamperska, 2D and 3D cell cultures - a comparison of different types of cancer cell cultures, Arch. Med. Sci. 14 (4) (2018) 910–919.

[18] R. Xie, V. Pal, Y. Yu, X. Lu, M. Gao, S. Liang, M. Huang, W. Peng, I.T. Ozbolat, A comprehensive review on 3D tissue models: biofabrication technologies and preclinical applications, Biomaterials 304 (2024) 122408.

[19] M.P. Lutolf, M. Radisic, J. Beekman, D.D. Huh, M. Huch, M.Y. Turco, Z. N. Tahmasebi Birgani, D. Gao, R. Yao, H. Lin, T. Takebe, In vitro human cell-based models: what can they do and what are their limitations? Cell 187 (17) (2024) 4439–4443.

[20] G. Lutzweiler, A. Ndreu Halili, N. Engin Vrana, The overview of porous, bioactive scaffolds as instructive biomaterials for tissue regeneration and their clinical translation, Pharmaceutics 12 (7) (2020).

[21] X. Zhang, X. Chen, H. Hong, R. Hu, J. Liu, C. Liu, Decellularized extracellular matrix scaffolds: recent trends and emerging strategies in tissue engineering, Bioact. Mater. 10 (2022) 15–31.

[22] A. Filipiak-Duliban, K. Brodaczewska, A. Kajdasz, C. Kieda, Spheroid culture differentially affects cancer cell sensitivity to drugs in melanoma and RCC models, Int. J. Mol. Sci. 23 (3) (2022) 1166.

[23] C. Angeli, J.P. Wroblewska, E. Klein, C. Margue, S. Kreis, Protocol to generate scaffold-free, multicomponent 3D melanoma spheroid models for preclinical drug testing, STAR Protocol. 5 (2) (2024).
[24] A.L. Harris, S.E. Lee, L.K. Dawson, L.A. Marlow, B.H. Edenfield, W.F. Durham, T. J. Flotte, M. Thompson, D.L. Small, A.J. Synnott, S.N. Markovic, J.A. Copland, Targeting the cyclin dependent kinase and retinoblastoma axis overcomes standard of care resistance in BRAF V600E -mutant melanoma, Oncotarget 9 (13) (2017).
[25] G. Parmiani, Melanoma cancer stem cells: markers and functions, Cancers (Basel) 8 (3) (2016).
[26] B.J. Wilson, K.R. Saab, J. Ma, T. Schatton, P. Pütz, Q. Zhan, G.F. Murphy, M. Gasser, A.M. Waaga-Gasser, N.Y. Frank, M.H. Frank, ABCB5 maintains melanoma-initiating cells through a proinflammatory cytokine signaling circuit, Cancer Res. 74 (15) (2014) 4196–4207.
[27] J. Lee, A.A. Abdeen, J. Hedhli, K.L. Wycislo, I.T. Dobrucki, T.M. Fan, L. W. Dobrucki, K.A. Kilian, Melanoma topology reveals a stem-like phenotype that promotes angiogenesis, Sci. Adv. 3 (10) (2017) e1701350.
[28] J. Lee, A.A. Abdeen, K.L. Wycislo, T.M. Fan, K.A. Kilian, Interfacial geometry dictates cancer cell tumorigenicity, Nat. Mater. 15 (8) (2016) 856–862.
[29] J. Lee, T.G. Molley, C.H. Seward, A.A. Abdeen, H. Zhang, X. Wang, H. Gandhi, J. L. Yang, K. Gaus, K.A. Kilian, Geometric regulation of histone state directs melanoma reprogramming, Commun. Biol. 3 (1) (2020) 341.
[30] Y. Liu, S. Nemec, C. Kopecky, M.H. Stenzel, K.A. Kilian, Hydrogel microtumor arrays to evaluate nanotherapeutics, Adv. Healthc. Mater. 12 (14) (2023) 2201696.
[31] A. Yui, M.J. Oudin, The rigidity connection: matrix stiffness and its impact on cancer progression, Cancer Res. 84 (7) (2024) 958–960.
[32] Z. Mai, Y. Lin, P. Lin, X. Zhao, L. Cui, Modulating extracellular matrix stiffness: a strategic approach to boost cancer immunotherapy, Cell Death Dis. 15 (5) (2024) 307.
[33] M. Zhang, B. Zhang, Extracellular matrix stiffness: mechanisms in tumor progression and therapeutic potential in cancer, Exp. Hematol. Oncol. 14 (1) (2025) 54.
[34] C.T. Mierke, Extracellular matrix cues regulate mechanosensing and mechanotransduction of cancer cells, Cells 13 (1) (2024) 96.
[35] E.A. Seftor, N.V. Margaryan, R.E.B. Seftor, M.J.C. Hendrix, Heterogeneity of melanoma with stem cell properties, Adv. Exp. Med. Biol. 1139 (2019) 105–114.
[36] A.J. Nirmal, Z. Maliga, T. Vallius, B. Quattrochi, A.A. Chen, C.A. Jacobson, R. J. Pelletier, C. Yapp, R. Arias-Camison, Y.A. Chen, C.G. Lian, G.F. Murphy, S. Santagata, P.K. Sorger, The spatial landscape of progression and immunoediting in primary melanoma at single-cell resolution, Cancer Discov. 12 (6) (2022) 1518–1541.
[37] J.J. Grob, M.M. Amonkar, B. Karaszewska, J. Schachter, R. Dummer, A. Mackiewicz, D. Stroyakovskiy, K. Drucis, F. Grange, V. Chiarion-Sileni, P. Rutkowski, M. Lichinitser, E. Levchenko, P. Wolter, A. Hauschild, G.V. Long, P. Nathan, A. Ribas, K. Flaherty, P. Sun, J.J. Legos, D.O. McDowell, B. Mookerjee, D. Schadendorf, C. Robert, Comparison of dabrafenib and trametinib combination therapy with vemurafenib monotherapy on health-related quality of life in patients with unresectable or metastatic cutaneous BRAF Val600-mutation-positive melanoma (COMBI-v): results of a phase 3, open-label, randomised trial, Lancet Oncol. 16 (13) (2015) 1389–1398.
[38] C. Robert, J.J. Grob, D.L. Stroyakovskiy, B. Karaszewska, A. Hauschild, E. Levchenko, V. Chiarion Sileni, J. Schachter, C. Garbe, I. Bondarenko, H.J. Gogas, M. Mandalà, J.B.A.G. Haanen, C. Lebbé, A.A. Mackiewicz, P.L. Rutkowski, P. D. Nathan, A. Ribas, M.A. Davies, K.T. Flaherty, P. Burgess, M. Tan, E. Gasal, M. Voi, D. Schadendorf, G.V. Long, Five-year outcomes with dabrafenib plus trametinib in metastatic melanoma, N. Engl. J. Med. 381 (7) (2019) 626–636, https://doi.org/10.1056/NEJMoa1904059. Epub 2019 Jun 4.
[39] G.V. Long, K.T. Flaherty, D. Stroyakovskiy, H. Gogas, E. Levchenko, F. de Braud, J. Larkin, C. Garbe, T. Jouary, A. Hauschild, V. Chiarion-Sileni, C. Lebbe, M. Mandalà, M. Millward, A. Arance, I. Bondarenko, J. Haanen, J. Hansson, J. Utikal, V. Ferraresi, P. Mohr, V. Probachai, D. Schadendorf, P. Nathan, C. Robert, A. Ribas, M.A. Davies, S.R. Lane, J.J. Legos, B. Mookerjee, J.J. Grob, Dabrafenib plus trametinib versus dabrafenib monotherapy in patients with metastatic BRAF V600E/K-mutant melanoma: long-term survival and safety analysis of a phase 3 study, Ann. Oncol. 28 (7) (2017) 1631–1639.
[40] V. Atkinson, G.V. Long, A.M. Menzies, G. McArthur, M.S. Carlino, M. Millward, R. Roberts-Thomson, B. Brady, R. Kefford, A. Haydon, J. Cebon, Optimizing combination dabrafenib and trametinib therapy in BRAF mutation-positive advanced melanoma patients: guidelines from Australian melanoma medical oncologists, Asia Pac. J. Clin. Oncol. 12 (S7) (2016) 5–12.
[41] D.W. Huang, B.T. Sherman, R.A. Lempicki, Systematic and integrative analysis of large gene lists using DAVID bioinformatics resources, Nat. Protoc. 4 (1) (2009) 44–57.
[42] B.T. Sherman, M. Hao, J. Qiu, X. Jiao, M.W. Baseler, H.C. Lane, T. Imamichi, W. Chang, DAVID: a web server for functional enrichment analysis and functional annotation of gene lists (2021 update), Nucleic Acids Res. 50 (W1) (2022) W216–w221.
[43] M. Ashburner, C.A. Ball, J.A. Blake, D. Botstein, H. Butler, J.M. Cherry, A.P. Davis, K. Dolinski, S.S. Dwight, J.T. Eppig, M.A. Harris, D.P. Hill, L. Issel-Tarver, A. Kasarskis, S. Lewis, J.C. Matese, J.E. Richardson, M. Ringwald, G.M. Rubin, G. Sherlock, Gene ontology: tool for the unification of biology. The Gene Ontology Consortium, Nat. Genet. 25 (1) (2000) 25–29.
[44] M.V. Christensen, C.K. Høgdall, K.M. Jochumsen, E.V.S. Høgdall, Annexin A2 and cancer: a systematic review, Int. J. Oncol. 52 (1) (2018) 5–18.
[45] Y. Ning, Y. Li, H. Wang, ANXA2 is a potential biomarker for cancer prognosis and immune infiltration: a systematic pan-cancer analysis, Front. Genet. 14 (2023).
[46] K. Van Bortle, D.P. Marciano, Q. Liu, T. Chou, A.M. Lipchik, S. Gollapudi, B. S. Geller, E. Monte, R.T. Kamakaka, M.P. Snyder, A cancer-associated RNA polymerase III identity drives robust transcription and expression of snaR-A noncoding RNA, Nat. Commun. 13 (1) (2022) 3007.
[47] Z.Q. Wang, Z.X. Wu, Z.P. Wang, J.X. Bao, H.D. Wu, D.Y. Xu, H.F. Li, Y.Y. Xu, R. X. Wu, X.X. Dai, Pan-cancer analysis of NUP155 and validation of its role in breast cancer cell proliferation, migration, and apoptosis, BMC Cancer 24 (1) (2024) 353.
[48] M. Rossi Sebastiano, G. Konstantinidou, Targeting long chain acyl-CoA synthetases for cancer therapy, Int. J. Mol. Sci. 20 (15) (2019).
[49] M. Ilmer, B.W. Renz, F. Kühn, M. Drefs, D. Koliogiannis, J. Werner, T. Kirchner, D. Horst, C. Woischke, PBXIP1 – an indicator for poor outcome and metastatic spread in colorectal cancer, Pathol. Res. Pract. 236 (2022) 153993.
[50] L. Crisafulli, M. Brindisi, M.G. Liturri, C. Sobacchi, F. Ficara, PBX1: a TALE of two seasons—key roles during development and in cancer, Front. Cell Dev. Biol. 12 (2024).
[51] W. Chen, J. Dong, J. Haiech, M.C. Kilhoffer, M. Zeniou, Cancer stem cell quiescence and plasticity as major challenges in cancer therapy, Stem Cells Int. 2016 (2016) 1740936.
[52] S. Bruschini, G. Ciliberto, R. Mancini, The emerging role of cancer cell plasticity and cell-cycle quiescence in immune escape, Cell Death Dis. 11 (6) (2020) 471.
[53] K.A. Heslop, V. Milesi, E.N. Maldonado, VDAC modulation of cancer metabolism: advances and therapeutic challenges, Front. Physiol. 12 (2021) 742839.
[54] M. Liu, X. Yang, Patient-derived xenograft models: current status, challenges, and innovations in cancer research, Genes Dis. 12 (5) (2025) 101520, https://doi.org/10.1016/j.gendis.2025.101520.
[55] M. Hidalgo, F. Amant, A.V. Biankin, E. Budinská, A.T. Byrne, C. Caldas, R. B. Clarke, S. de Jong, J. Jonkers, G.M. Mælandsmo, S. Roman-Roman, J. Seoane, L. Trusolino, A. Villanueva, Patient-derived xenograft models: an emerging platform for translational cancer research, Cancer Discov. 4 (9) (2014) 998–1013.
[56] Society for Melanoma Research 2012 Congress, Pigm. Cell Melanoma Res. 25 (6) (2012) 836–903.
[57] J.R. Tse, A.J. Engler, Preparation of hydrogel substrates with tunable mechanical properties, Curr. Protoc. Cell Biol. 47 (1) (2010) 10.16.1–10.16.16.
[58] X. Tang, M. Yakut Ali, M.T.A. Saif, A novel technique for micro-patterning proteins and cells on polyacrylamide gels, Soft Matter 8 (27) (2012) 7197–7206.
[59] S. Zaqout, L.-L. Becker, A.M. Kaindl, Immunofluorescence staining of paraffin sections step by step, Front. Neuroanat. 14 (2020).
[60] A. Keller, A.I. Nesvizhskii, E. Kolker, R. Aebersold, Empirical statistical model to estimate the accuracy of peptide identifications made by MS/MS and database search, Anal. Chem. 74 (20) (2002) 5383–5392.
[61] A.I. Nesvizhskii, A. Keller, E. Kolker, R. Aebersold, A statistical model for identifying proteins by tandem mass spectrometry, Anal. Chem. 75 (17) (2003) 4646–4658.